

Fig. 1 Two sequential SIMS depth profiles of a 1500Å poly Si on 1000Å Si oxide sample display good repeatability between all elements except for H. The same element in the two sequential profiling is labelled with the same color. All elements are in raw ion counts. The e-beam was applied to overcome the sample charging effects arising from 1000Å Si oxide underneath of the poly Si films

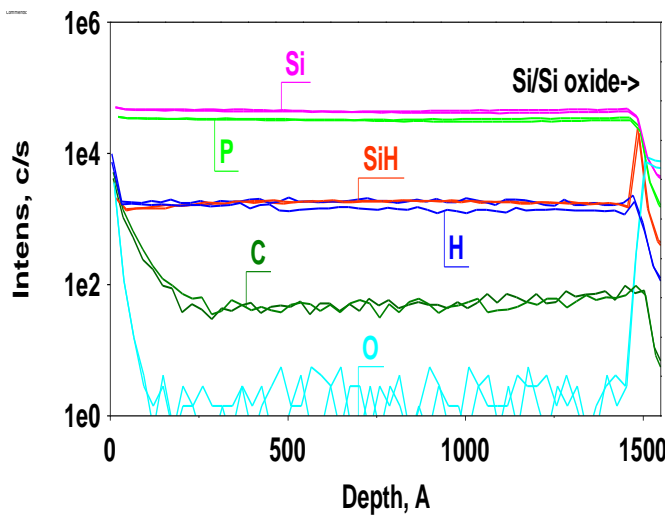


Fig. 2 Two sequential SIMS depth profiles of H, C, O, P, and Si on a 1500Å poly Si on 1000Å Si oxide sample show good repeatability C, O, Si, and P ion signals. H arising from SiH<sup>-</sup> cluster ions repeat well, but H arising from H<sup>-</sup> atomic ions do not repeat. The same element in the two sequential profiling is labelled with the same color. All element signals are plotted in raw ion counts *vs.* depth. The O depth profiles are noisy since they are derived from monitoring <sup>18</sup>O and not <sup>16</sup>O, and <sup>16</sup>O is saturated in the Si oxide layer on the bottom. The e-beam was applied to overcome the sample charging effects arising from 1000Å Si oxide underneath of the poly Si films

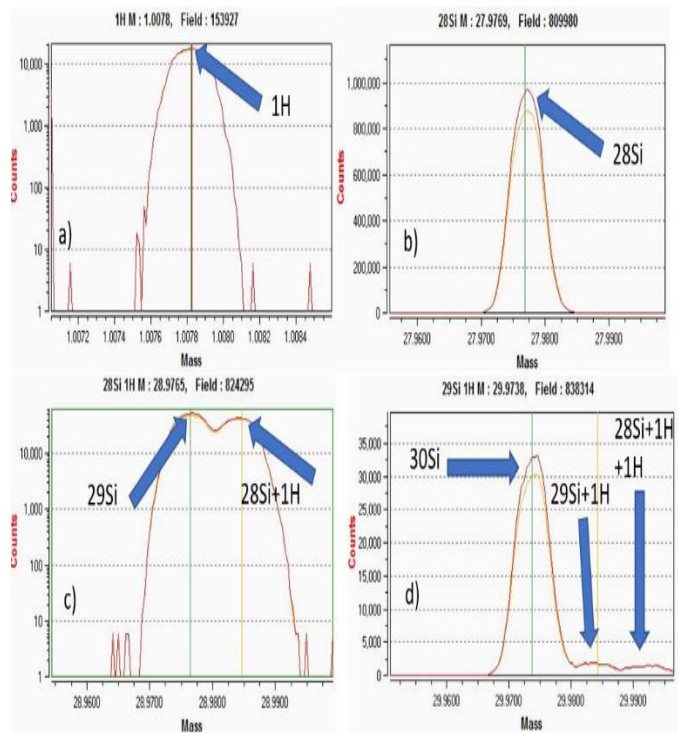


Fig. 3 Mass spectral calibration of H<sup>-</sup>, Si<sup>-</sup>, and SiH<sup>-</sup> ion intensities collected on a Si sample with ~4000 HMR, showing good mass separations between <sup>28</sup>SiH<sup>-</sup> and <sup>29</sup>Si, as well as <sup>29</sup>SiH<sup>-</sup> mass separation from <sup>30</sup>Si<sup>-</sup> and <sup>28</sup>SiH<sub>2</sub><sup>-</sup>.

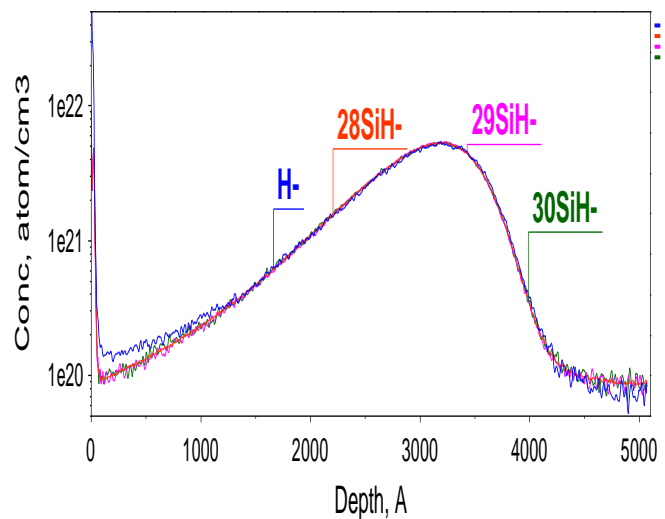


Fig. 4 Overlay of H depth profiles by monitoring both atomic H<sup>-</sup>, and <sup>28</sup>SiH<sup>-</sup>, <sup>29</sup>SiH<sup>-</sup>, and <sup>30</sup>SiH<sup>-</sup> cluster ions on H<sub>2</sub>.8keV6.8E16 implant in Si sample. The ~4000 HMR was applied during the analysis.

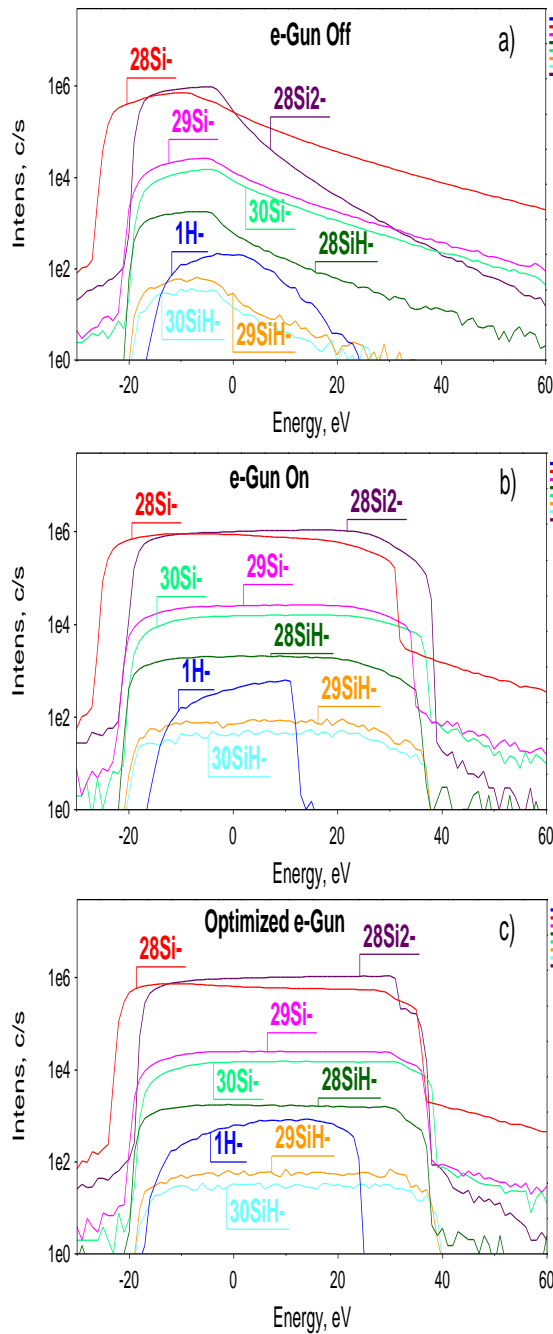


Fig. 5 Comparison of the  $\text{H}^-$  atomic ion,  $\text{SiH}^-$  cluster ion, and Si matrix ion energy distributions, acquired with identical 1keV  $\text{Cs}^+$  impacting ion beam sputtering at negative secondary ion polarity of 3keV, (a) e-gun off, (b) e-gun on, and (c) optimized e-gun conditions including adjusting e-beam position. The e-gun charge compensation with 3keV and current density  $40 \text{ } (\mu\text{A}/\text{m}^2)$ . All atomic and cluster ion energy distribution bands were collected as a function of the sample voltage offsets from -30eV to 60eV on same  $1500\text{Å}$  poly Si on  $1000\text{Å}$  Si oxide sample. The intensities are in arbitrary units for comparison purposes only. Figs. 5 (a, b, c) indicate that the e-beam charge compensation results in large differences in the ion energy distribution bands for these atomic and cluster ions.

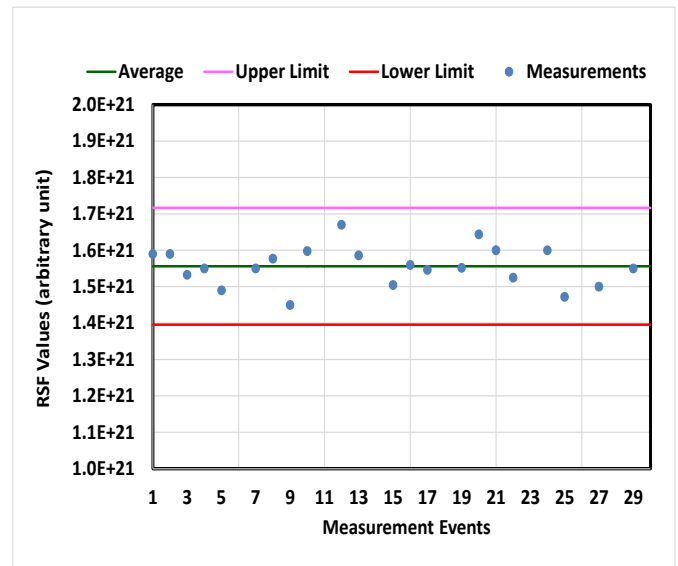


Fig. 6 Long-term data of the H RSF from analysis of the H implant in Si laboratory standard reference, taken by monitoring  $\text{SiH}^-$  ions with respect to Si matrix under  $\text{Cs}^+1\text{KeV}$  impacting. Limits are within  $\pm 3\sigma$ . RSF values are plotted in arbitrary unit.

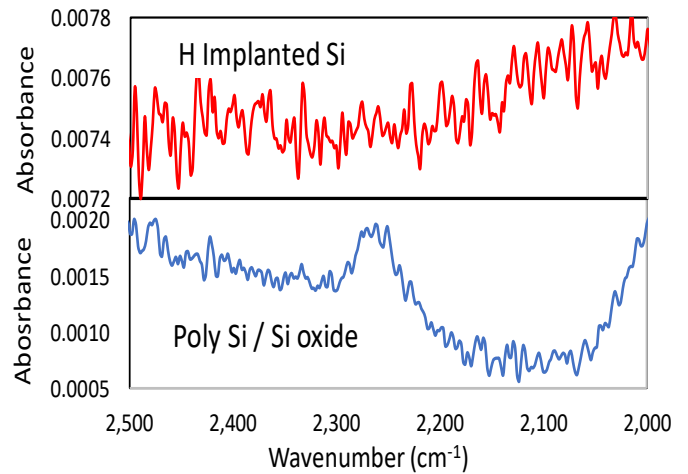


Fig. 7 FTIR spectrum consists of 256 co-added scans that have had both ATR and baseline corrections applied. No evidence of Si-H stretching bands occur in the  $2280\text{cm}^{-1} - 2000\text{cm}^{-1}$  region on  $\text{H}2.8\text{keV}6.8\text{E}16$  implant in Si sample, and a small peak around  $2260\text{cm}^{-1}$  on  $1800\text{Å}$   $2\text{E}21 \text{ H}$  ( $\text{ats}/\text{cm}^3$ ) poly Si on  $1\text{kÅ}$  Si oxide sample.